Structure of Supercritically Dried Calcium Silicate Hydrates (C-S-H) and structural Changes Induced by Weathering

Victor Morales-Florez[a,b*], Nicolas de la Rosa-Fox[c]

a- Instituto de Ciencia de Materiales de Sevilla (ICMS, CSIC-Universidad de Sevilla). Av. Américo Vespucio 49, 41092, Sevilla (Spain)

b- Departamento de Física de la Materia Condensada, Facultad de Física, Universidad de Sevilla. Av. Reina Mercedes s/n, Sevilla, 41012 (Spain)

c- Departamento de Física de la Materia Condensada, Facultad de Ciencias, Universidad de Cádiz. Av. Republica Saharaui s/n 11510 Puerto Real, Cadiz (Spain)

Abstract

The nanostructure of supercritically dried calcium silicate hydrates was researched. This particular drying procedure was used to avoid nanostructure modifications due to conventional drying processes. Thus, in this work, the as-precipitated cementitious C-S-H structure was obtained for the first time. A specific surface area 20% larger than conventionally dried C-S-H was measured. Given the importance of this nanostructured phase for the properties of hydrated cements, especially when in contact with CO_2-rich environments, the supercritically dried C-S-H was weathered for two weeks. The structural effects of this weathering process on the C-S-H were researched and calcium carbonate microcrystal precipitation or the presence of silica by-product are reported. Calcite and aragonite polymorphs were observed, as well as nanoporous silica forming globular arrangements. In addition, two weeks of weathering was not enough to carbonate the entire C-S-H sample.

Introduction

Despite cementitious construction materials are known and used for millennia, the nanostructure of their main binding phase, calcium silicate hydrate (C-S-H)* [1] is not completely understood yet. C-S-H is a porous particulate quasi-mineral of variable composition which is formed by the hydration of the C_2S and C_3S phases of the cement. It plays a central role in the properties of hydrated cements, such as mechanical properties or durability of the cementitious buildings. Moreover, the reactivity of hydrated cements with carbon dioxide, such as atmospheric (weathering effect) or from carbon capture geological storage, also depends on this calcium-rich phase [2, 3]. Consequently, it is crucial to evaluate the properties of hydrated cements when exposed to CO_2 [4-6] and specially to understand the structural changes due to carbonation.

There is some controversy on the structure of this porous phase given the heterogeneity in particle shape and in the chemical composition of the C-S-H phase. The scientific community has assumed the coexistence of two types of C-S-H depending on where they precipitate with respect to the parent anhydrous C_xS grains, namely, in the pore space among the original clinker grains or in the space initially occupied by them. This binary description has been described as low density C-S-H (LD) and high density (HD), respectively [1, 7-9]†. LD C-S-H is a broad, low dense phase with sheet-like and needle-like particle morphologies, whereas HD C-S-H is a

* Cement notation: C:CaO; S:SiO_2; H:H_2O. The hyphenation shows variable composition.

† In cement science, there are several classifications for the different types of C-S-H, namely, outer product (OP) and inner product (IP), C-S-H Type I and Type II, etc. In this work, we do fall into a discussion on these classifications, but remark on the complexity of the nanostructure.

rough and denser disordered particulate matrix. Transmission electron microscopy (TEM) imaging clearly illustrates the aforementioned types of C-S-H [10].

These nanostructures can be described as assemblages of random packings of nanocrystalline particles several nanometres in size, arranged in several hierarchical levels, where embedded water molecules can be found [9-13]. This phase eventually extends through the space between resting non-reacted mineral grains [14]. Small angle scattering experiments (SAXS if x-rays are used as radiation, or SANS if neutrons are used) have been performed to research C-S-H structure during hydration of the cement [15], reporting the surface fractal morphology of C-S-H [16] eleven hours after the hydration of cement on a length scale of 10-100 nm. These experiments also revealed some characteristic features such as the multi-level nature of the structures, the density and the role of water in the basic building blocks [17, 18]. In fact, size, shape, crystallographic nature, water content and their arrangements forming hierarchical fractal structures, have been the focus of several research works, both experimentally [19-21] and computationally [13,22]. Tobermorite or jennite are being proposed as their crystallographic and chemical nature [10, 23].

Regarding the reactivity with CO_2, studies on the structural changes of cementitious calcium-rich phases due to carbonation have previously shown that ~50 nm clusters and pores with radii between 2 nm and 7 nm appear under the influence of different environments containing CO_2 [24], mainly due to the carbonation of the low-density C-S-H [25]. Fast carbonation due to atmospheric CO_2 has been reported [26], especially for calcium-to-silica ratio over 0.75 [27]. However, no significant change in the specific surface area has been observed [28].

In this work, a new technique for obtaining and studying cementitious C-S-H was used, and a new perspective on the structural research of this important binding

nanoporous material is proposed. It has been stated for almost a century that the drying process of nanoporous structures leads to the collapse of the structure itself, given the huge interpore forces that appear due to the surface tension of the liquid-gas interface that are inversely proportional to pore radius. To avoid these huge tensions, the liquid-gas interphase should be avoided when removing the solvent. This is achieved by raising temperature and pressure over the critical point of the solvent (243 ºC and 63 bar for ethanol) and then removing it under supercritical conditions [29]. Typically, hydrated cement samples and synthetic C-S-H are necessarily dried to perform research based on several characterisation techniques (TEM, SEM, nitrogen physisorption, typical SAXS or SANS experiments). Consequently, the C-S-H structure that has been studied is not the same as was precipitated in the original aqueous phase, prior to drying. In this work, we have used the supercritical drying process to obtain and study the C-S-H structure, not dramatically affected by the conventional drying process. To our knowledge, this is the first time that the study of the original as-precipitated nanostructure of C-S-H has been performed under dry conditions.

Materials and methods

Synthesis and weathering

The C-S-H sample was synthesised from a solution with a Ca/Si molar ratio of 1.8 according to the co-precipitation method [30] which consists of adding, under stirring, a solution of Na_2SiO_3 (Merck, 1L = 1.35 kg) to a calcium saturated solution (a completely transparent solution of CaO, [Ca] ~18 mM). This solution was aged for up to 21 days in sealed containers inside an N_2-filled glovebox at ambient pressure and temperature. In

this inert environment, the supernatant was exchanged with CO_2-free water to remove Na traces and to avoid carbonation during precipitation. This washing yielded a Na content in the final solid phase down to 1% wt. (X-ray fluorescence, AXIOS PANalytical instrument). Afterwards, the water was exchanged by ethanol, and then ethanol was exchanged three times daily for 4 days to remove the water. Some minor structural changes may appear due to the solvent exchange, but they are known to be negligible so the obtained structures will be representative of the precipitated "frozen" C-S-H. The sample was placed into an autoclave and heated up to 250ºC and 72 bar. Then, the ethanol was vented off under supercritical conditions, namely, releasing pressure isothermally at 250ºC. The complete drying process lasted 5 hours. The autoclave was opened inside a nitrogen-filled glovebox and the supercritically dried C-S-H was obtained. One part of the sample was weathered, that is, it was put in contact with the atmosphere for 2 weeks (room temperature and ~40% RH) so the atmospheric CO_2 could react to form calcium carbonate.

Two different samples were studied: the original supercritically dried C-S-H, labelled scCSH, always handled with care so as to not allow it to come into contact with atmospheric CO_2 to avoid weathering, and the sample that was weathered for two weeks, labelled wscCSH.

Characterisation techniques

Phase characterisation was done by X-ray diffraction (XRD). Nitrogen physisorption, small angle x-ray scattering (SAXS), energy dispersive spectrometry (EDX) and scanning electron microscopy (SEM) were used for nanostructure investigations. To keep the scCSH sample safe from atmospheric gases for XRD and

SAXS analyses, it was placed between two polyester films hermetically sealed and mounted on sample holders inside the N_2-filled glovebox. XRD analyses were performed on a diffractometer (Philips X'Pert) with Cu-Kα radiation, from 5.00° to 70.00° with a step of 0.05° and counting time of 80 s. SAXS experiments were performed in a device with Cu-Kα radiation and a 2 theta step of 0.01º (Philips X'Pert PANalytical). This way, the covered *q*-range was 0.004 – 0.356 $Å^{-1}$.

Likewise, the original sample scCSH was placed inside the nitrogen physisorption sample holder inside the glovebox. Nitrogen physisorption experiments (Micrometrics, model ASAP2010) were made at a constant temperature of 77.35 K. Isotherm curves were analysed by the Brunauer-Emmet-Teller [31] and Barret-Joyner-Halenda [32] methods to obtain the specific surface area (S_{BET}) and pore size distribution (PSD), respectively. The scCSH sample was degasified by heating at different temperatures from 100 to 250ºC, under a nitrogen flux for two hours, to explore the role of adsorbed water in this nanostructure. The wscCSH sample was degasified at 100ºC. SEM and EDX were performed using a SEM-FEG (Hitachi S480) with an acceleration voltage of 2kV. The time of contamination due to atmospheric gases was minimised to <15 s, as the sample was mounted on the SEM sample holder inside the glove box. Thereby, the scCSH sample was in contact with the atmosphere only for the time it took to be placed inside the SEM vacuum chamber and to pump down the system.

Results and Discussion

Once the supercritical drying process was finished and the autoclave was opened inside the nitrogen-filled glovebox, an extremely fine and volatile fluffy powder was obtained. The XRD analyses of this scCSH powder (Figure 1) showed the presence of

broad weak peaks of poorly crystallized tobermorite (PDF file: 00-029-0331) characteristic of C-S-H. No phase other than tobermorite was precipitated, that is, no portlandite (calcium hydroxide) nor jennite, nor calcium carbonate phases were observed. On the other hand, the weathering of the wscCSH was firstly confirmed by XRD. In Figure 2, the x-ray diffraction pattern shows the presence of different calcium carbonate polymorphs, calcite (PDF number: 00-001-0837) and aragonite (PDF number: 01-071-2396), together with some resting tobermorite. The precipitation of aragonite was already observed in C-S-H samples that were carbonated with no extra water [33], similar to our carbonation conditions where only atmospheric humidity is wetting the sample. Thus, in two weeks, the weathering of the original C-S-H was not completed, given the presence of resting tobermorite.

The nanostructure of the scCSH was researched first by nitrogen physisorption. With a gentle degasifying procedure, at T = 100ºC for 2h, similar specific surface areas S_{BET} = 447 m^2/g and t-Plot external surface S_{tPlot}= 433 m^2/g were measured. All the structural features of the different experiments are summarised in Table 1. This measured surface area was significantly higher (~20% or more) than others reported for synthetic C-S-H, tobermorite, or hydrated cement pastes [1, 13, 34], typically between 30 m^2/g and 378 m^2/g. Therefore, the actual C-S-H structure that exists in the aqueous media after hydration of the cement and prior to drying presents higher specific surface than those typically observed by conventional procedures. Consequently, hydrated cements will be more reactive than theoretically expected. A pore volume of 0.913 cm^3/g and a wide pore size distribution (PSD) was obtained, with a constant mesopore population between 10 nm and 40 nm (Figure 3, top). Then, a monotonic increase in the pore size population from 10 nm towards lower radii was observed, increasing very rapidly below 5 nm, but without any well-defined pore size peak. In other words, this

PSD showed the presence of two levels of porosity: an important pore population below 5 nm formed by the packing of the elemental structural elements, and another important mesopore population formed by their hierarchical arrangement. The PSD can be explained by randomly arranged particles forming two different hierarchical levels. Nevertheless, no well-defined typical pore radius was observed (no peak is observed), indicating a very heterogeneous population of particle sizes and shapes. The elemental building blocks forming C-S-H that have been reported in the literature as microcrystals with sizes around ~5 nm [18, 35] were also present in this supercritically dried sample, forming the observed porosity below 5 nm. Therefore, they were not affected by the drying process and structural differences between the conventionally dried and supercritically dried C-S-H have to be explained in terms of changes on higher structural hierarchical levels.

Considering the skeleton density ρ_{sk} = 2.4 g/cm^3 similar to tobermorite, the maximum specific surface area that could be obtained would be ~500 m^2/g, close to that measured in the scCSH. Therefore, the conventional drying process induces shrinkage of the globules formed by the arrangement of the elemental building blocks by bringing them together, but not shrinkage of the building blocks themselves. In addition, a bulk density of ρ_{bulk} = 0.75 g/cm^3 and a porosity P = 68.7% could be derived for the scCSH. This density is lower than the density of the C-S-H found in hydrated cements, between 1.4 – 2.0 g/cm^3 [1, 23], indicating that the obtained supercritically dried C-S-H could be a frozen initial stage of the common C-S-H, prior to structure maturing and shrinkage produced by conventional drying.

The role of the adsorbed water in the C-S-H nanostructure was researched by changing the degasifying temperature. Nitrogen physisorption experiments were performed on the original C-S-H degasified at 175ºC and 250ºC, in addition to 100ºC

(discussed before). The structural parameters obtained with different degasifying temperatures are summarised in Table 1, and plotted versus degassing temperature in Figure 3, bottom. Instead of an increase in the specific surface area due to the release of interstitial water, a significant decrease of this parameter was observed, indicating shrinkage of the structure. Typical C-S-H structural models [7-9, 13, 18] have always considered a certain amount of low-bonded interstitial or intraglobular water, adsorbed or encapsulated among the basic building blocks of the structure. These results indicate that releasing this water leads to the collapse of the structure, showing the structural effects of the drying process of these nanostructured samples. This way, the specific surface area S_{BET} decreases to 360 m^2/g at a degassing temperature of 175ºC and to 282 m^2/g at 250ºC. Moreover, supercritical drying of the C-S-H did not provoke this collapse of the structure, and it was kept invariable up to the degassing process. The porous volume presented a similar behaviour to specific surface area, supporting the idea of shrinkage of the structure. However, the hierarchical distribution of the pores does not disappear despite the shrinkage, and the three PSD curves for the three different temperatures show constant shape (Figure 3, top), with an slight decrease in the pore population below 5 nm with degassing at 175 ºC, followed by a decrease of the pore population between 10 and 30 nm when rising temperature up to 250 ºC.

On the other hand, the weathered sample presented much lower specific surface area values than any of the original samples (Table 1). Carbonation of C-S-H yields calcium carbonate crystals and silica by-products. The silica by-product is an amorphous silica gel with a high specific surface area and nanometric particle size, but the calcium carbonate crystals, as aragonite or calcite, are expected to form micrometric crystals with very low specific surface area values, thus decreasing the value of the entire sample. Finally, the relative decrease of the pore volume was significantly lower,

indicating a larger average particle size but more spread out thanks to the contribution of the silica gel.

The scanning electron microscopy micrographs of the scCSH sample showed a random arrangement of flake-like or sheet-like structures, typical of tobermorite (Figure 4, top). The size of these flakes was quite heterogeneous, circa 20 nm wide and 200 nm long. This flake-like morphology has been associated to outer product (or low density) C-S-H [10] in coherence with the derived bulk density values discussed before. Thus, using this synthesis route and this drying procedure, synthetic low density C-S-H could be precipitated. In addition, some thin stick morphologies around 400 nm long and 20 nm thick could also be seen (upper left corner of Figure 4, top, and Figure 4, bottom). These stick morphologies have been previously reported in samples synthesised at 170ºC [36]. So, the presence of stick-like morphologies could be an artefact due to the heat-treatment of the supercritical drying process.

The different morphologies of the weathering by-products can be seen in Figures 5, 6 and 7. In Figure 5, branched calcite microcrystals can be seen instead of typical rhombohedral calcite crystals. The absence of silica on these microcrystals (confirmed by EDX) supported this identification. The size of the crystals indicated a small specific surface area value, so the disappearance of C-S-H flakes and the precipitation of these large calcite crystals decreased the bulk specific surface area of the sample. In Figure 6, a branch of calcium carbonate sticks is shown. This morphology has been associated with aragonite [37]. In the background of Figures 5 and 6, remaining C-S-H flakes can be observed, showing the incomplete carbonation of C-S-H, so the mere exposure to atmospheric CO_2 under room conditions yielded a partially carbonated sample. Finally, in Figure 7, the silica by-product is shown. It precipitated as a hierarchical arrangement of pseudo-spherical particles. In this figure, 200 nm sized aggregates of silica particles

are shown, but smaller structural elements (< 50 nm) similar to those sizes previously reported [24] can also be seen. EDX tests were made on these arrangements to measure the calcium-to-silica ratio, and to discard other phases than silica. The obtained values of Ca/Si = 0.40 ± 0.04 supports the identification of this phases as the silica by-product. Therefore, the precipitation of this amorphous silica by-product contributes to maintaining high specific surface area values of the weathered sample, and a small average pore radius as well (15.8 nm), typically formed by the aggregation of elemental silica particles.

The structural features of the scCSH and those changes due to weathering were researched by SAXS as well [38]. The obtained intensities are plotted in Figure 8. First, the absence of a well-defined Guinier range in the scCSH was remarkable and indicated the absence of a well-defined size and shape of scatterers. The shape of the curve indicated a very heterogeneous particle size and shape distribution. Nevertheless, there was a change in the slope of the log-log plot, and the $q_1^{crossover}$ value indicated a typical size of the scatterers of 3.2 nm. In this case, considering Babinet's Principle, scattering may be caused by the pores among the elemental nanocrystalline building blocks usually characterised as ~5 nm size [18, 35]. In addition, the scattering curve of the original sample increased its intensity towards low *q*-values, revealing the existence of larger (> 100 nm) typical sizes of the scatterers, which may correspond to the size of the flakes. However, the covered *q*-range in these experiments was not sufficient to resolve this large structural feature. Both linear regimes of the log-log plot of the scattering curve covered much less than one decade, so the slope of these regimes could not be consistently associated to any fractal description.

On the other hand, the intensity curve of the wscCSH sample showed a Guinier range at low *q*-values, with a derived Guinier's radius of 14.3 nm (28.6 nm particle size),

similar to the characteristic size of 29.6 nm derived from the $q_2^{crossover}$. These new structural elements that appear after the weathering process are identified with silica by-product particles (Figure 7), as silica gel is usually well-described by spherical particles and well-resolved by small angle scattering and Guinier's model [39, 40]. In addition, the previously reported $q_1^{crossover}$ could be also observed, corresponding to the persistence of some ~3.2 nm sized scatterers among the resting nanocrystalline building blocks, as the C-S-H had not been completely weathered.

Conclusions

The synthetic C-S-H sample dried by the supercritical drying process presented a greater specific surface area and pore volume than the conventionally dried C-S-H. The differences between conventionally and supercritically dried CSH are explained in terms of the shrinkage of the structure due to conventional drying. In this regard, the reactive surface of the C-S-H when in an aqueous paste was ~20% larger than that usually measured in conventionally dried C-S-H.

The exposure of the sample to atmospheric CO_2 under room conditions is enough to the carbonate the sample, but 2 weeks of weathering yielded a partially carbonated sample. SEM images and XRD analysis confirmed the precipitation of calcite and aragonite. Finally, the hierarchical distribution of the precipitated silica gel by-product, with ~28 nm typical particle size arranged in globules of ~200 nm size was observed.

Acknowledgements

The authors are grateful to the Consejería de Innovación Ciencia y Empresa of the Junta de Andalucía (Spain) for supporting this work with the annual grant TEP115. This

work was possible thanks to the technical staff of the Instituto de Ciencia de Materiales de Sevilla (ICMS, CSIC-US). VMF thanks the CSIC for financial support through the JAE-Doc programme.

References

1 Taylor HFW (1997) Cement Chemistry. Thomas Telford Publishing, London.

2 Barlet-Gouédard V, Rimmelé G, Porcherie O, Quisel N, Desroches J (2009) Int J Greenh Gas Control 3:206

3 Jaramillo P, Griffin WM, McCoy ST (2009) Environ Sci Technol 43(21):8027

4 Rimmelé G, Varlet-Gouédard V, Porcherie O, Goffé B, Brunet F (2008) Cem Concr Res 38:1038

5 See for example: GRASP project (http://www.grasp-co2.eu) or CO2Sink project (http://www.co2sink.org). Last visit: Sept 21st, 2012.

6 Corvisier J, Brunet F, Fabbri A, Bernard S, Findling N, Rimmelé G, Barlet-Gouédard V, Beyssac O, Goffé B (2010) Eur J Mineral 22:63

7 Feldman RF, Sereda PJ (1970) Eng J Can 53:53

8 Jennings HM (2000) Cem Concr Res 30:101

9 Jennings HM (2008) Cem Concr Res 38:275

10 Richardson IG (2004) Cem Concr Res 34:1733

11 Frattini E, Chen SH, Baglioni P, Bellissent-Funel MC (2001) Phys Rev E 64:020201

12 Popova A, Geoffroy G, Gartner EM, Lapp A (2002) J Am Ceram Soc 85:1303

13 Morales-Flórez V, Brunet F (2009) Molecular Simulation 35:1001

14 Lloyd RR, Provis JL, Van Deventer JSJ (2009) J Mater Sci 44:620

15 Mazumder S, Sen D, Patra AK, Khadilkar SA, Cursetji RM, Loidl R, Baron M, Rauch H (2005) Phys Rev B 72:224208

16 Mazumder S, Sen D, Bahadur J, Klepp J, Rauch H, Teixeira J (2010) Phys Rev B

82:064203

17 Thomas JJ, Jennings HM, Allen AJ (1998) Cem Concr Res 28:897

18 Allen AJ, Thomas JJ, Jennings HM (2007) Nat Materials 6:311

19 Blinc R, Lahajnar G, Zummer S (1988) Phys Rev B 38:2873

20 Thomas JJ, Allen AJ, Jennings HM (2008) J Am Ceram Soc 91:3362

21 Skinner LB, Chae SR, Benmore CJ, Wenk HR, Monteiro PJM (2010) Phys Rev Lett 104:195502

22 Manzano H, Ayuela A, Dolado JS (2007) J Comp. Aided Mater Des 14:45

23 Gonzalez-Teresa R, Morales-Florez V, Manzano H, Dolado JS (2010) Materiales de construccion 60:7

24 Häussler F, Palzer S, Eckart A, Hoell A (2002) Appl Phys A 74:s1124

25 Morales-Florez V, Brunet F (2012) J Mater Sci 47:764

26 Garbev K, Stemmermann P, Black L, Breen C, Yarwood J (2007) J Am Ceram Soc 90:900

27 Black L, Garbev K, Gee I (2008) Cem Concr Res 38:745

28 Johannesson B, Utgennant P (2001) Cem Concr Res 31:925

29 Kistler S. Coherent Expanded-Aerogels (1932) J Phys Chem 36(1):52

30 Sugiyama D, Fujita T (2006) Cem Concr Res 36:227

31 Brunauer S, Emmett PH, Teller E (1938) J Am Chem Soc 60:309

32 Barret EP, Joyner LG, Halenda PP (1951) J Am Chem Soc 73:373

33 Shtepenko O, Hills C, Brough A, Thomas M (2006) Chem Eng J 118:107

34 Siauciunas R, Rupsyte E, Kitrys S, Galeckas V (2004) Coll And Surf A 244:197

35 Xu Z, Viehland D (1996) Phys Rev Lett 77:952

36 Rossler C, Stark J, Steiniger F, Tichelaar W (2006) J Am. Ceram. Soc **89**:627

37 Gobac ZZ, Posilović H, Bermanec V (2009) Geologia Croatica 62(3):201

38 Glatter O, Kratky O (1982) Small Angle X-Ray Scattering. Academic Press, London

39 De la Rosa-Fox N, Morales-Flórez V, Toledo-Fernández JA, Piñero M, Esquivias L, Keiderling U (2008) J Sol-Gel Sci and Tech 45:245

40 Woignier T, Reynes J, Hafidi Alaoui A, Beurroies I, Phalippou J (1998) J of Non-Cryst Solids 241:45

TABLES AND FIGURE CAPTIONS

Tables

Table 1. Nitrogen physisorption results for the scCSH and the wscCSH degasified at different temperatures. For derived bulk density and porosity values, tobermorite density has been considered as the skeleton density.

Figures

Figure 1. X-ray diffraction pattern (Cu-Kα radiation) of the scCSH.

Figure 2. X-ray diffraction pattern (Cu-Kα radiation) of the wscCSH.

Figure 3. Top, pore size distributions of the scCSH obtained for different degassing temperatures. Bottom, dependence of texture parameters (specific surface area S_{BET} and porous volume Vp) on degassing temperature for the scCSH sample.

Figure 4. Scanning electron micrographies of the scCSH sample.

Figure 5. Scanning electron micrography of the wscCSH sample.

Figure 6. Calcium carbonate microcrystals of the wscCSH observed by SEM.

Figure 7. Silica gel by-product observed in the weathered wscCSH sample.

Figure 8. SAXS intensities of both scCSH and wscCSH samples. The intensities were normalised for comparison purposes.

Table 1

Degassing temperature (ºC)	S_{BET} (m^2/g)	S_{tPlot} (m^2/g)	<Rp> nm	Vp (cm^3/g)	ρ_{bulk} (g/cm^3)	Porosity (%)
Original sample						
100	447	433	7.5	0.913	0.752	68.7
175	360	329	6.5	0.686	0.907	62.2
250	282	277	6.8	0.567	1.017	57.6
Weathered sample						
100	166	160	15.8	0.587	0.996	58.5

Figure 1
Click here to download high resolution image

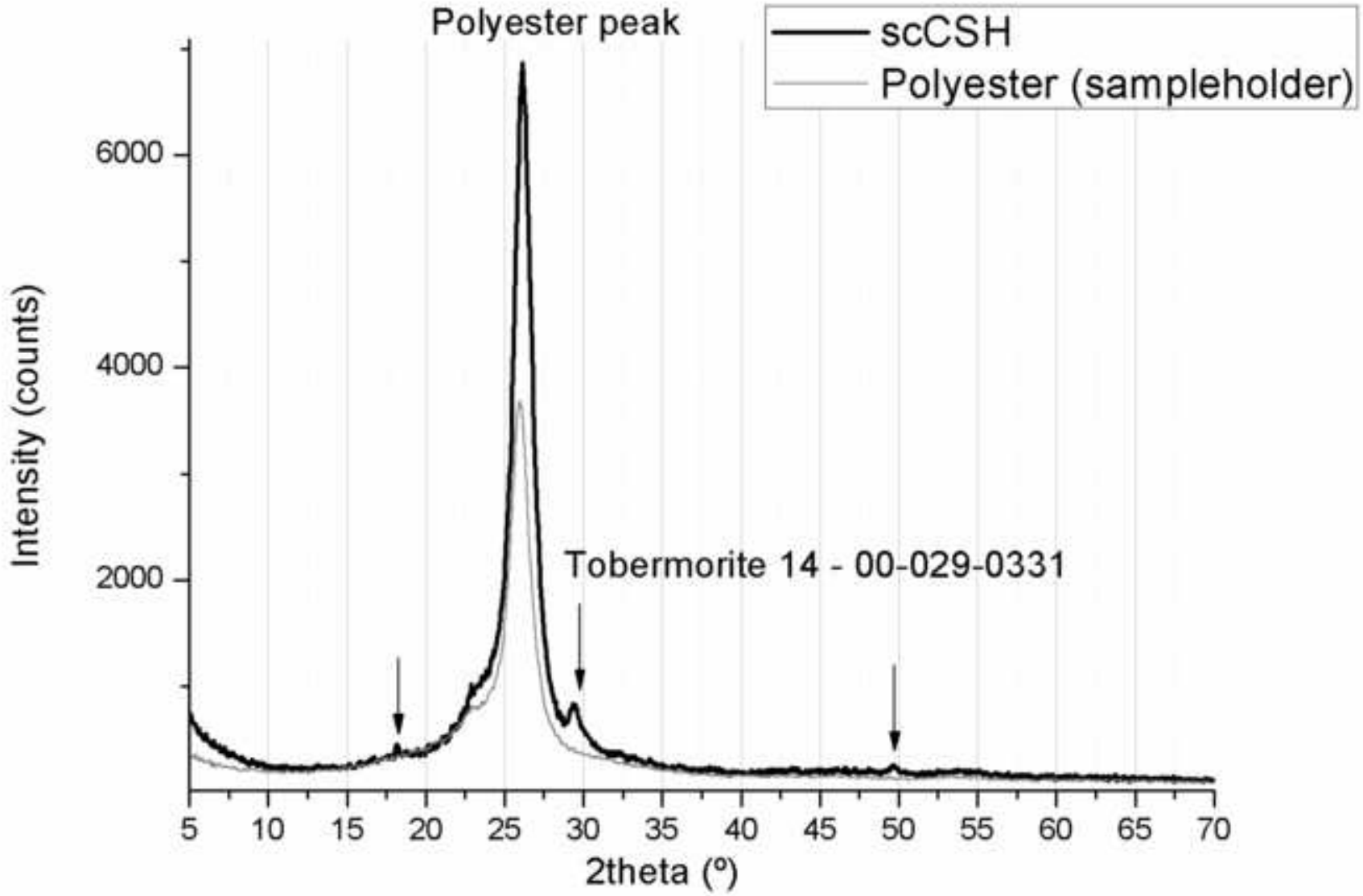

Figure 2
Click here to download high resolution image

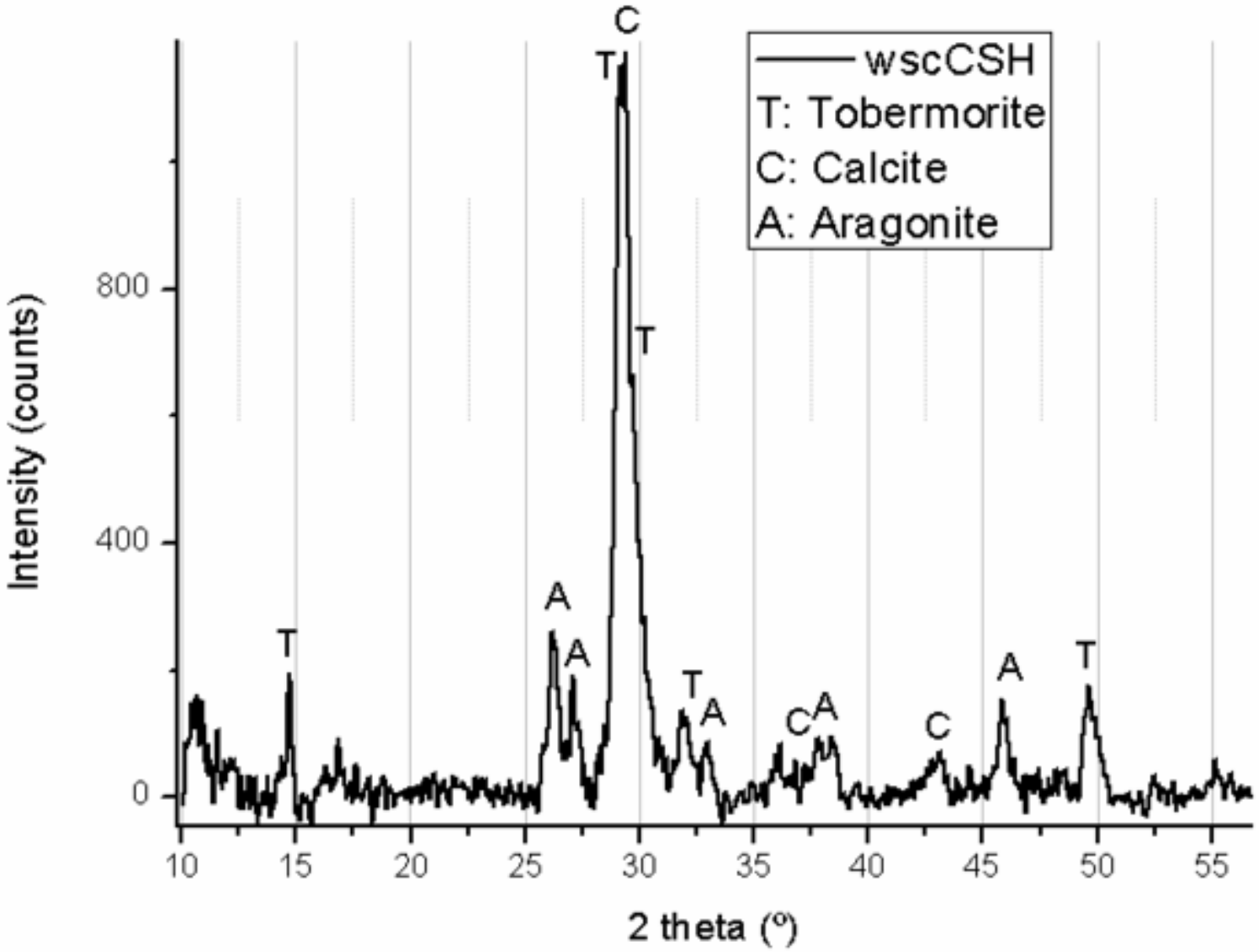

Figure 3
Click here to download high resolution image

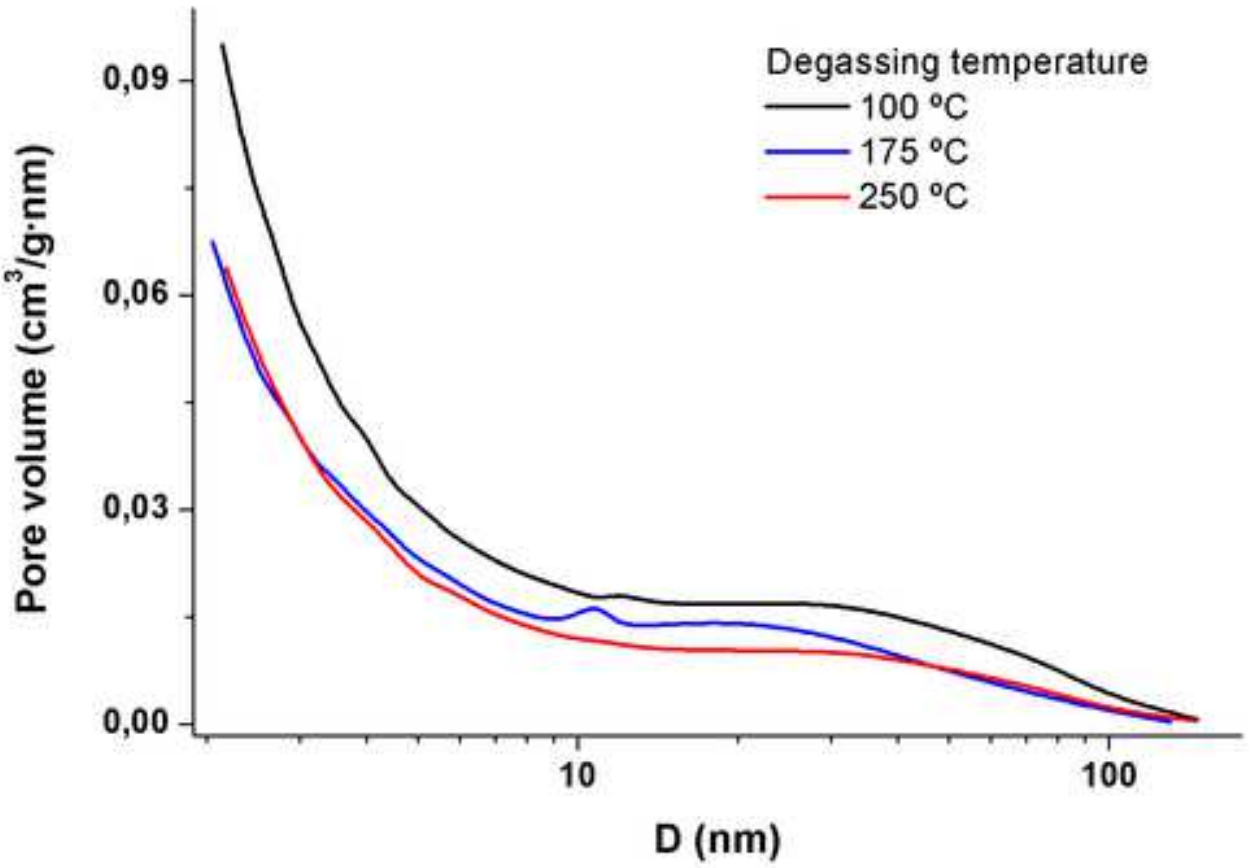

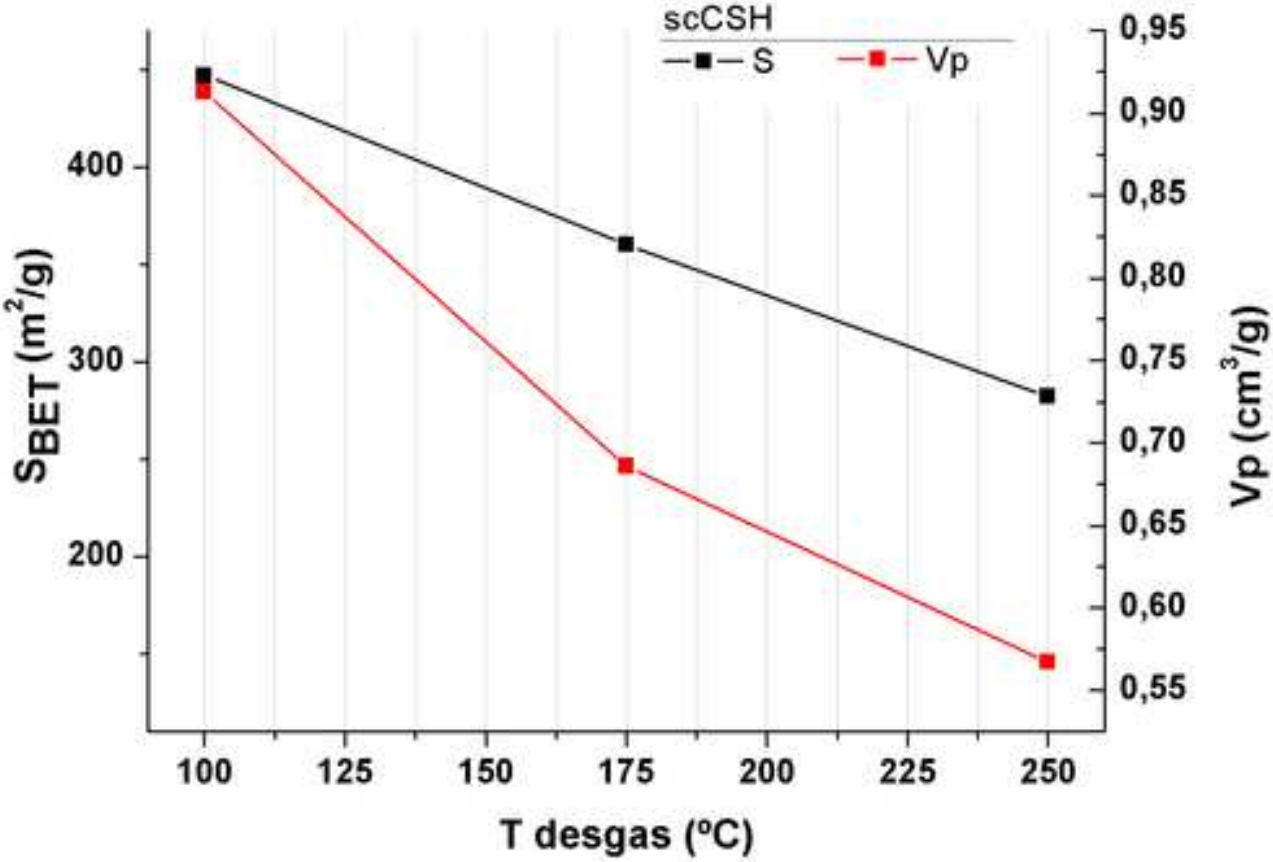

Figure 4
Click here to download high resolution image

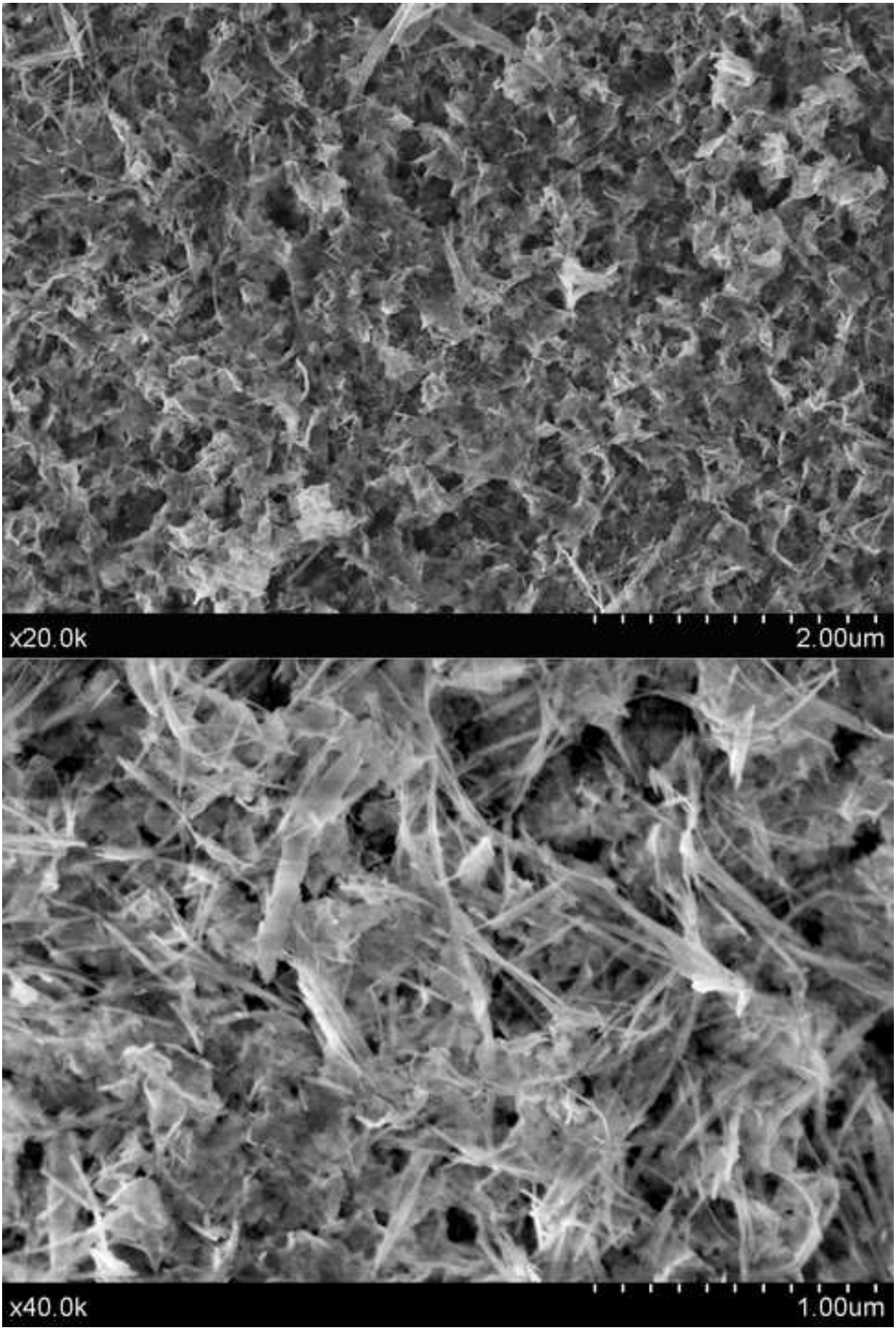

Figure 5
Click here to download high resolution image

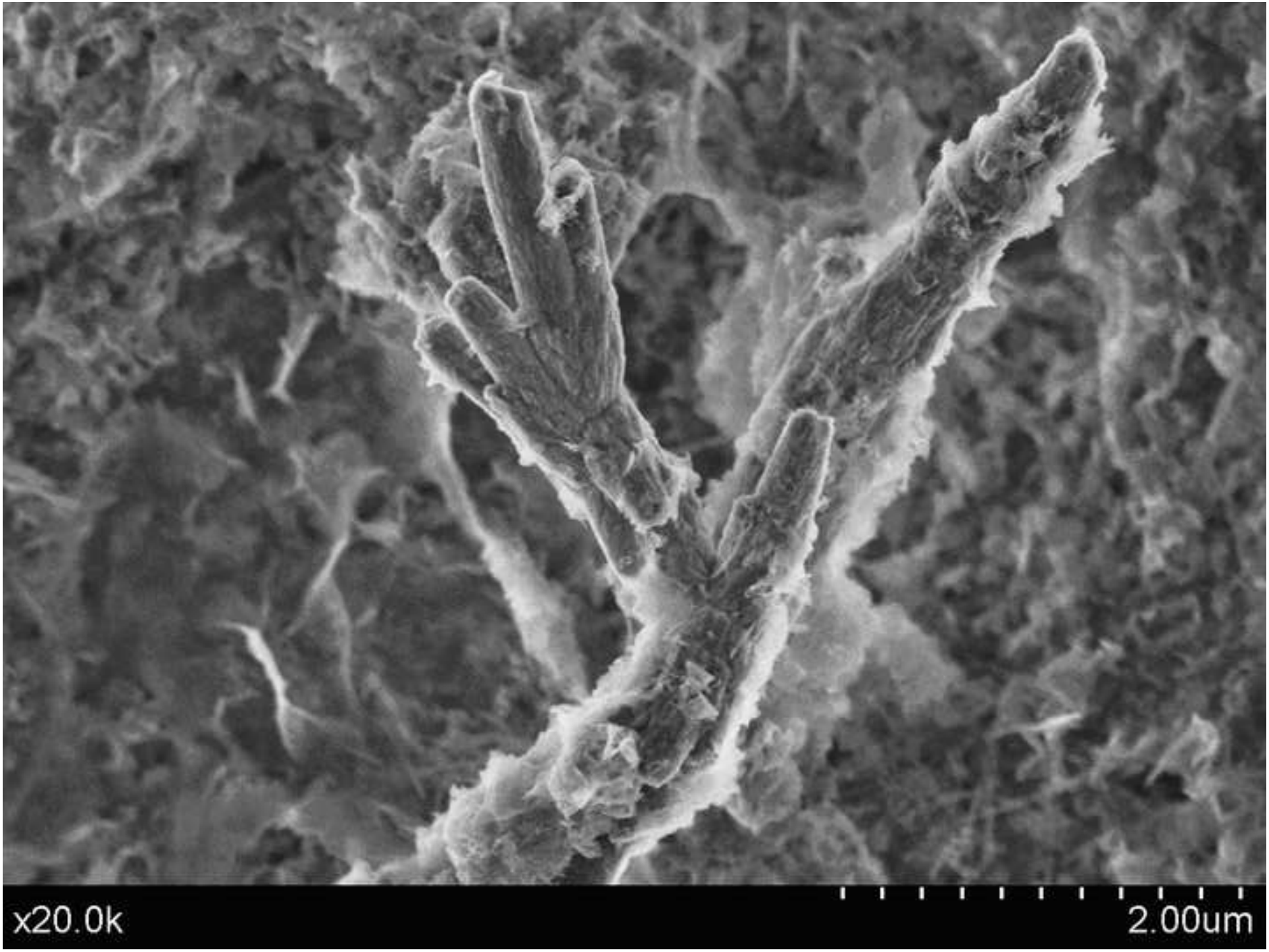

Figure 6
Click here to download high resolution image

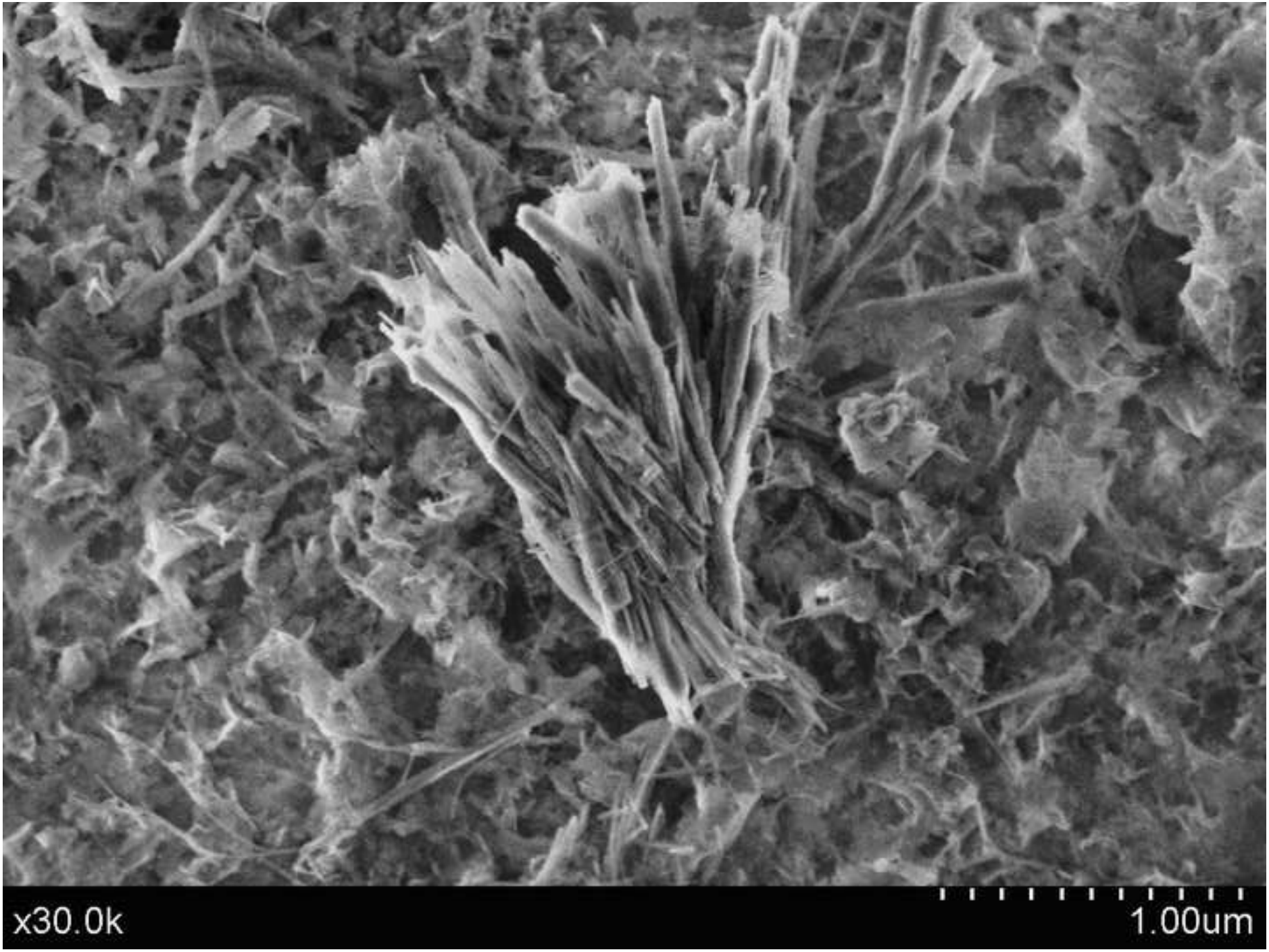

Figure 7
Click here to download high resolution image

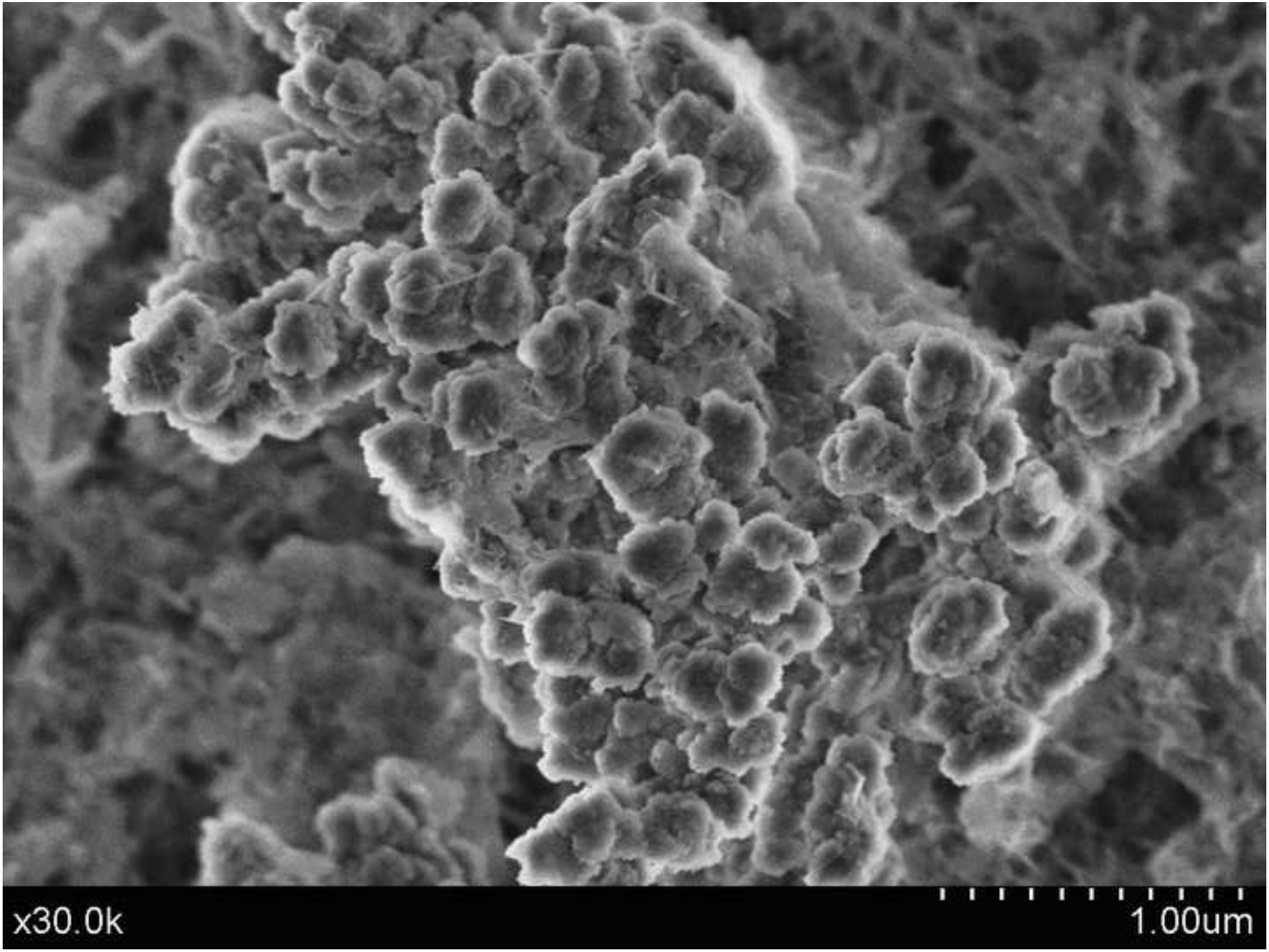

Figure 8
Click here to download high resolution image